Quasielastic light scattering in rutile, ZnSe, silicon, and $SrTiO_3$

A. Koreeda, T. Nagano, S. Ohno, and S. Saikan
Department of Physics, Graduate School of Science, Tohoku University, Sendai 980-8578, Japan
(Received 31 August 2004; revised manuscript received 30 September 2005; published 13 January 2006)

Quasielastic light scattering (QELS) has been investigated in the crystals of TiO_2 (rutile), ZnSe, silicon, and $SrTiO_3$. The temperature dependence of the linewidth for the QELS has been measured in detail by backward light scattering interferometry and by impulsive stimulated thermal scattering technique in the temperature range from 5 to 670 K. The quasielastically scattered spectra observed consist of two components, which can be classified into two types, namely, types I and II, depending on the linewidth. The analyses have shown that the linewidth of the QELS I changes from the well-known q^2 to a q^1 dependence with either decreasing temperature or increasing q, where q is the wave-vector transfer in the scattering experiment. It has been found that the linewidth of the QELS I in arbitrary phonon regimes including "hydrodynamic," "collisionless," and "intermediate" can be roughly estimated solely in terms of average sound velocity and the "phonon Knudsen number" $q\bar{l}$, where $\bar{l}$ is the mean free path of thermal phonons. A broad doublet spectrum, which was first reported by Hehlen *et al.* in Phys. Rev. Lett. **75**, 2416 (1995), has been observed in $SrTiO_3$ at low temperatures, and its origin has been also discussed in terms of phonon Knudsen number.

DOI: 10.1103/PhysRevB.73.024303 PACS number(s): 78.35.+c, 63.20.−e, 66.30.Xj, 77.90.+k

I. INTRODUCTION

Quasielastic light scattering (QELS), which is often alternatively referred to as the "central peak" phenomenon, appears in Rayleigh-Brillouin spectra in many crystalline dielectrics, and has captured considerable attention in spectroscopy due to the relationship with phase transitions.[1–10] The high-performance interferometer[11] has encouraged observations of QELS in dielectric crystals,[3,4] and a number of mechanisms responsible for the spectra in a variety of frequency ranges have been reviewed:[5,8] QELS may arise from a number of origins and often two or more of these are active in a single material at the same time.

While QELS is often associated with critical phenomena, it has been observed not only in the materials that exhibit phase transitions,[5–9,12] but also in those which are considered to be unrelated to phase transitions, such as silicon[4,13] or diamond.[14] Furthermore, it has been found that the spectra consist of two quasielastic components, which have temperature and wave-vector dependences common in a number of materials.[12–17] We refer to the narrower and the broader QELS components as types I and II, respectively, in this paper. The QELS I had been just considered as arising due to diffusive entropy fluctuations before it was pointed out that entropy fluctuation was not appropriate for the origin of the QELS at low temperatures.[13–15] In that case, nondiffusive (nonthermodynamic) "two-phonon difference scattering" must be considered as a lowest order approximation, and it has succeeded in explaining the behavior of the QELS I at low temperatures qualitatively and semiquantitatively.[15] The two phonon difference scattering predicts a linear-in-q dependence for the type-I linewidth, where q is the wave-vector transfer, in contrast to the well-known q^2 dependence due to diffusive entropy fluctuations. However, there seems to have been little discussion on the consistency between the two frameworks or on the transition from one to the other from both theoretical and experimental points of view. Also, it is suggested that the QELS I can never extend out to the Brillouin peaks,[15] and the QELS II is often observed coupling to the Brillouin peaks giving rise to asymmetric Brillouin line shapes.[9,17] These imply that along with the well-known intensity relation, the so-called Landau-Placzek relation,[18,19] there should be an undiscussed and unrevealed connection between Brillouin scattering and the two QELS components concerning their frequency and wave vector.

In this paper, we investigate the frequency and wave-vector dependences of QELS in crystals of TiO_2 (rutile), ZnSe, silicon, and $SrTiO_3$ with continuously changing phonon regimes from hydrodynamic to collisionless. In rutile, we extend the temperature range up to 670 K in order to investigate the transition of the phonon regime from hydrodynamic to collisionless in more detail than in the previous report.[15] In $SrTiO_3$ and silicon, although the two component QELS has been already pointed out,[12,16] the temperature dependence of the linewidth of the QELS I has not been given so far. In addition to the conventional light scattering technique, we have made use of impulsive stimulated thermal scattering (ISTS),[20] which is a technique utilizing laser-induced dynamic gratings:[21] while the former enables unequilibrated, "collisionless" phonon regime, the latter realizes equilibrated "hydrodynamic" phonon regime. The intermediate regime between the two limiting phonon regimes has been achieved by changing temperature. We analyze the linewidths of both types of QELS normalizing by the Brillouin frequency in each sample, and show that there is a common relation between the linewidth of the QELS I and the Brillouin frequency in all the samples investigated. Transition from quadratic to linear dependence on q for the type-I linewidth has been found in some of the samples, and we discuss the consistency between the hydrodynamic and collisionless phonon regimes.

In Sec. II, we review the theoretical background concerning QELS in crystals, and introduce the "phonon Knudsen number." Also we reconsider the mean free path (MFP) of

phonons in detail. Experimental details are described in Sec. III, and the results for both backscattering and ISTS are presented in Sec. IV. In Sec. V, we discuss the relation between the QELS and the Brillouin frequency in each of the phonon regimes introducing an average Brillouin frequency.

II. THEORETICAL BACKGROUND

A. The phonon Knudsen number and phonon regimes

Let us consider light scattering in a crystal. When the temperature of the crystal is high and the number of phonons is sufficiently large, phonon collisions occur frequently and local thermal equilibrium is well established. In this case, it can be considered that the incident light is scattered by fluctuations in temperature (or equivalently in entropy). This "thermal" light scattering leads to a diffusive Rayleigh central peak, which is often called entropy-fluctuation light scattering (EFLS).[22] It is well known that the linewidth [half width at half maximum (HWHM)] of EFLS is given as $\Gamma_{\mathrm{EFLS}}=D_{\mathrm{th}}q^2$, where D_{th} is the thermal diffusivity and q is the magnitude of the transferred wave vector. This condition for the heat transport theory to be valid is often referred to as the "collision-dominated" or "hydrodynamic phonon regime."[13,14] In the opposite limit, where phonons rarely collide, phonon transport theory is no longer valid and temperature or entropy cannot be defined locally. In this case, nonthermodynamic scattering processes must be taken into account, and we should rather consider that light is scattered as a consequence of simultaneous creation and annihilation of a few phonons (two-phonon difference light scattering).[6,13–15] This limiting condition is often referred to as the "collisionless phonon regime." In general cases between the two regimes, however, neither the phonon hydrodynamics nor the two-phonon scattering model is adequate: for this intermediate regime no light scattering theory is available so far to the best of our knowledge.

In general, the criterion for hydrodynamics to be valid for a system is determined whether $\bar{l}/\Lambda \ll 1$ or not, where $\bar{l}$ is the mean free path (MFP) of constituent particles and Λ is a characteristic length. This value $\bar{l}/\Lambda \equiv \mathrm{Kn}$ is called the "Knudsen number," which represents the reciprocal number of collision frequency over the length Λ. In terms of Kn, the criteria for the hydrodynamic, the intermediate, and the collisionless phonon regimes can be written as $\mathrm{Kn} \ll 1$, $\mathrm{Kn} \approx 1$, and $\mathrm{Kn} \gg 1$, respectively. Since the characteristic length scale in a light scattering experiment is defined by q^{-1}, the Knudsen number in a light scattering experiment for a phonon gas is defined as

$$\mathrm{Kn} = q\bar{l}. \tag{1}$$

We refer to Eq. (1) as the "phonon Knudsen number" hereafter. In light scattering experiments, q can be varied by changing the scattering angle θ since q is defined as

$$q = 2n\frac{2\pi}{\lambda}\sin\frac{\theta}{2}, \tag{2}$$

where n, λ, and θ represent the refractive index, the wavelength of the incident light, and the scattering angle, respectively. The MFP of phonons can be calculated from macroscopic quantities from the well-known relation that

$$D_{\mathrm{th}} = \frac{1}{3}\bar{v}\bar{l}, \tag{3}$$

where $\bar{v}$ is the mean sound velocity.[23] For $\bar{v}$ we adopt the Debye's mean velocity, viz., $\bar{v}^{-3}=(1/3)(v_{\mathrm{LA}}^{-3}+2v_{\mathrm{TA}}^{-3})$ with v_{LA} and v_{TA} being longitudinal and transverse acoustic velocities, respectively, and isotropy is also assumed for simplicity.

In any phonon regimes mentioned above, we can consider that light is scattered by the fluctuations in the phonon density in crystals.[5,7,8] Therefore, we can characterize light scattering due to phonon-density fluctuations by the phonon Knudsen number. The concept to characterize dielectric properties in terms of phonon Knudsen number is also becoming essential in studies of heat-transport in nanoscale structures,[24] where dimensions of sample are close to the MFP of phonons even at relatively high temperatures.

In a back-scattering configuration with a visible light source, q is of the order from 10^7 to 10^8 m^{-1}, while in a forward-scattering with a small scattering angle of $\lesssim 1°$, q can be reduced to a value of the order of less than 10^5 m^{-1}. Since $\bar{l}$ ranges from 10^{-9} to 10^{-4} m (Ref. 23) by changing temperature, we can, therefore, visit arbitrary phonon regimes from hydrodynamic ($q\bar{l} \ll 1$) to collisionless ($q\bar{l} \gg 1$), simply by changing the scattering angle θ or temperature. In a forward light scattering experiment, however, one usually encounters a difficulty in detecting the weak scattered light out of the intense source light, which propagates almost in the same direction as the signal light. However, a time-domain light scattering technique introduced by Nelson and co-workers[20,21] called impulsive stimulated thermal scattering (ISTS) can overcome the above difficulty. The ISTS can reduce θ to less than 1°, yielding a q of the order of 10^4 m^{-1} or smaller.

We have, thus, performed two kinds of experiment, one of which is the backward light scattering interferometry with $\theta \approx 180°$ and the other is the ISTS with $\theta \lesssim 1°$. In both measurements, the temperature was widely varied ranging from $T \sim \Theta_D/100$ to $T \gtrsim \Theta_D$, where Θ_D is the Debye temperature. The experimental details of these two methods will be described in Sec. III.

B. The mean free path of phonons

Here we should comment in detail on the MFP of phonons that we consider in this paper. It should be noted that $\bar{l}$ is the MFP for all of the thermally excited phonons, rather than that of a specific phonon mode with a specific frequency or wave vector. The MFP of acoustic phonons measured in Brillouin scattering spectroscopy,[25] say l_B, is obtained from the linewidth of the spectra, viz., $l_B=v_B/\Gamma_B$, where v_B and Γ_B are the velocity of the acoustic phonon and the linewidth of the Brillouin line, respectively; the amplitude of the acoustic wave is attenuated by $1/e$ when it travels a distance of l_{B}. The works on crystalline quartz,[25–28] for example, have revealed that l_B is longer than 10^{-4} m at room temperature, giving $ql_B \simeq 10^4$, indicating that the observed phonon does not undergo any

collision until it travels a distance of several hundred wavelengths even at relatively high temperatures. That is why we can observe sharp Brillouin peaks in solids even at high temperatures, but the fact that the observed Brillouin phonon is "collision-free" appears to contradict the fact that $q\bar{l} \ll 1$ at high temperatures. However, it can be shown that $q\bar{l} \ll ql_B$, or more simply, $\bar{l} \ll l_B$, is actually general for solids at relatively high temperatures, and then we find that the simultaneous existence of the collision-dominated EFLS and the collision-free Brillouin component at relatively high temperatures is, of course, physically consistent. We present a simple discussion on that point below.

We consider a relatively high temperature such that $T \gtrsim \Theta_D$, which is required for thermohydrodynamics to be always valid. According to Akhieser's theory,[29,30] the acoustic attenuation rate per unit time Γ_B for sufficiently high temperatures is given as

$$\Gamma_B = \frac{\gamma_G^2 C_V \bar{\tau}}{3\rho v_B^2} \omega_B^2 T = \frac{3\alpha_l^2 BT}{C_V} \omega_B^2 \bar{\tau}, \tag{4}$$

where $\gamma_G = 3\alpha_l B / C_V$ is the averaged Grüneisen constant, α_l is the linear thermal expansion coefficient, B is the bulk modulus, C_V is the heat capacity per unit volume, $\bar{\tau}$ is the relaxation time or mean free time for thermal phonons, i.e.,

$$\bar{\tau} = \frac{\bar{l}}{\bar{v}}, \tag{5}$$

ρ is the mass density, and ω_B is the angular frequency of the acoustic phonon observed in Brillouin scattering, i.e.,

$$\omega_B = q v_B. \tag{6}$$

The Rayleigh linewidth Γ_R at sufficiently high temperatures corresponds to Γ_{EFLS} as described in Sec. II A, so that

$$\Gamma_R = D_{\mathrm{th}} q^2 = \frac{1}{3} \bar{v} \bar{l} q^2 = \frac{1}{3} \left(\frac{\bar{v}}{v_B} \right)^2 \omega_B^2 \bar{\tau}, \tag{7}$$

where we have used Eqs. (3), (5), and (6). Equations (4) and (7) give a ratio of the linewidth of the Rayleigh component to that of the Brillouin as

$$\frac{\Gamma_R}{\Gamma_B} = \frac{1}{3} \left(\frac{\bar{v}}{v_B} \right)^2 \frac{C_V}{\alpha_l^2 BT}. \tag{8}$$

Assuming that α_l is of the order of 10^{-5} to 10^{-6} K^{-1}, which is typical for most solids at room temperature, and that $\bar{v}$ is close to v_B, we find that Γ_R / Γ_B has a value of order 10^2. Note that Γ_R / Γ_B does depend on temperature and that Γ_R and Γ_B are never proportional to each other despite the appearance of Eq. (8). In fact, Γ_R and Γ_B have opposite temperature dependences: on cooling, Rayleigh component broadens while Brillouin peaks sharpen.

Similar to Eq. (8), a relation between the phonon Knudsen number $q\bar{l}$ and a quantity ql_B is obtained:

$$(q\bar{l})(ql_B) \sim \frac{1}{3} \frac{\bar{v}}{v_B} \frac{C_V}{\alpha_l^2 BT}, \tag{9}$$

which gives a value of order 10^2 for ordinary solids. This indicates that $q\bar{l}$ and ql_B can differ by orders of magnitude if one of them is much smaller or much larger than a few tens. In fact, since $q\bar{l} \ll 1$ (hydrodynamic phonon regime), we see from Eq. (9) that $ql_B \gg 1$. For example, in crystalline quartz at room temperature, the right-hand side of Eq. (9) gives $C_V / (3\alpha_l^2 BT) \sim 300$ with $\alpha_l = 8.5 \times 10^{-5}$ K^{-1},[31] $B \approx c_{11} = 9.4 \times 10^{10}$ Pa,[27] and $T = 300$ K. On the other hand, from the reported Brillouin linewidth[27] and thermal diffusivity,[32,33] and using a typical value of $q \approx 5 \times 10^7$ m^{-1}, $q\bar{l}$ and ql_B can be estimated to be ~ 0.15 and ~ 2300, respectively. These yield $(q\bar{l})(ql_B) \sim 350$, which is in good agreement with the value calculated by Eq. (9). Thus, we may regard that Eq. (9) can give a reasonable quantitative relation between $\bar{l}$ and l_B in hydrodynamic phonon regime.

The fact that l_B is much longer than $\bar{l}$ can be interpreted that the frequencies of the phonons participating in Rayleigh and Brillouin scattering differ by orders of magnitude. Brillouin scattering is considered to be due to the first order Raman process or "single particle scattering," in which a phonon with momentum $\hbar \boldsymbol{q}$ and energy $\hbar \omega_B$ is picked up. In contrast, Rayleigh scattering of light is considered to be due to second or higher order Raman processes, which involve two or more Umklapp phonons in the whole Brillouin zone.[5,13–15,34] Therefore, the frequency of the phonons that predominantly contribute to the Rayleigh scattering extends to $\sim \omega_D = k_B \Theta_D / \hbar \sim 10^{13}$ rad/s, which is several hundred times higher than ω_B, where ω_D is the Debye frequency. Since the higher is the frequency of a phonon the more strongly it undergoes attenuation,[68] such high-frequency "Rayleigh phonons" have much shorter MFP than that of low-frequency Brillouin phonons. It is also important to point out that the shorter the free path, the more effectively it contributes to thermal resistance (or, equivalently, reduces thermal conductivity). For example, a phonon collision after a free flight of a length L has a thousand times smaller contribution than a collision after $1/1000L$ flight. In fact, we obtain an effective attenuation of these two successive collisions as $L_{\mathrm{eff}}^{-1} = 1/L + 1000/L \approx 1000/L$. Therefore, the MFP estimated from Eq. (3) or Γ_{EFLS} should effectively reflect the contributions from the shortest free paths of phonons. Since the density of states for the zone boundary phonons are much higher than those for the zone center phonons, the phonon collisions at relatively high temperatures are considered to be dominated by the phonons in the zone boundary. Thus, $\bar{l}$ should be contributed largely from the zone-boundary phonons, resulting in a much shorter $\bar{l}$ than l_B.

While l_B has ω and q dependences, $\bar{l}$ does not essentially have frequency and wave-vector dependences because $\bar{l}$ is considered to be obtained by averaging for all the phonons in the whole Brillouin zone for the crystal. Although the MFP of each phonon does have ω and q dependences as one could obtain from "one-phonon" scattering experiments such as Brillouin scattering, one cannot find such strong ω and q

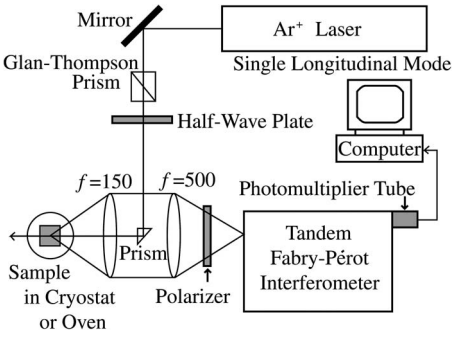

FIG. 1. Experimental setup for backscattering ($\theta=180^{\circ}$).

dependences in a zone-averaged MFP, i.e., in $\bar{l}$. Since l_B depends not only on temperature but also on frequency and wave vector, it is not appropriate that we define the Knudsen number of phonon gas in terms of l_B. The phonon Knudsen number $q\bar{l}$ is considered to properly characterize the length scale of the phonon gas because $\bar{l}$ depends basically only on temperature, i.e., only on phonon occupation number. It should be added that l_B is never inversely proportional to $\bar{l}$ despite the appearance of Eq. (9). Instead, l_B and $\bar{l}$ should have a similar temperature dependence because both of them are inversely proportional to the occupation number of thermal phonons essentially. From the above discussions, it is concluded that the simultaneous existence of the collision-dominated Rayleigh (EFLS) and the collision-free sharp Brillouin lines at relatively high temperatures is consistent.

III. EXPERIMENTAL

A. Backscattering experiment

In the backscattering experiments, a Sandercock-type tandem Fabry-Pérot interferometer[6] was employed. The experimental setup is depicted in Fig. 1. The dark counting rate of the photomultiplier tube (Hamamatsu R464-S) was measured to be approximately 0.8 counts per second on average without a cooler. The focal length and the aperture of the focusing/collecting lens was 150 and 50 mm, respectively, giving an F number of 3.0, which gave less than 2/3 the collection efficiency that reported by Stoddart and Comins.[16]

The free spectral range (FSR) of the interferometer was varied from 10 to 300 GHz, which was obtained from mirror spacings ranging from 1.5 to 0.05 cm, and the finesse was more than 55. Effect of higher order transmission in a Sandercock-type interferometer, which has been reported recently,[35–37] can cause a "knee" in combining the spectra obtained in different FSRs, and use of interference filters has been suggested for obtaining correct spectral line shapes in decades of frequency range. Although we have not utilized such compensation techniques, we consider that our analyses suffer little because we have not analyzed the "combined" spectra but have analyzed those obtained in one FSR in the least-squares fit. Thus artifactual spectral "knees" are not considered to be present in our analysis although the reported transmission effect may still give a constant background,[36] which can be reasonably taken into account by adding a baseline parameter in the least-squares fit.

The samples investigated were crystals of TiO_2 (rutile), ZnSe, silicon, and $SrTiO_3$ crystals because we found that the intensities of the QELS were strong enough to investigate the temperature variations.[17] Wehner and Klein have introduced solid state enhancement factor for the Rayleigh component as[22]

$$R_{\mathrm{WK}} = R_{\mathrm{LP}}(1-r)^2,$$

where R_{LP} is the Landau-Placzek ratio and r is the enhancement parameter defined as

$$r \equiv -\frac{\left(\frac{\partial n}{\partial T}\right)_u}{\alpha_V\left(\frac{\partial n}{\partial u}\right)_T},$$

where u is strain and α_V is the volume expansion coefficient. We have found that the values of $(1-r)^2$ in the materials we have investigated are relatively large; 260 for rutile, >48 for ZnSe, and 45 for $SrTiO_3$. We have not given the value for silicon because the photoelastic constants and temperature coefficient of refractive index for visible wavelength were not available.[69] The relatively large enhancement for the Rayleigh component can be ascribed to the fact that $(\partial n/\partial T)_u$, the temperature coefficient of refractive index at constant strain (i.e., without being accompanied by thermal expansion), in these materials is relatively large.[38–40] Note that literature values of temperature coefficients of refractive index are usually measured at constant pressure, so they include both pure thermo-optic effect and that just due to thermal expansion.[22] The contribution from thermal expansion can be estimated to be $-p\alpha_l$,[22] where p is an average photoelastic constant, and this has a value of the order of -10^{-7} 1/K. The pure thermo-optic coefficient $(\partial n/\partial T)_u$ in rutile at room temperature has been estimated to be -1.3×10^{-4}/K,[31,38,41] which is even twice as large as that of "quantum-paraelectric" $SrTiO_3$ at the same temperature.[40] It is important to note that the sign of $(\partial n/\partial T)_u$ in the above two materials is negative while that in ZnSe is positive. The negative sign of $(\partial n/\partial T)_u$ in rutile and $SrTiO_3$ is due to the fact that these two materials are "incipient ferroelectrics," which are dielectrics with weak ferroelectriclike nature. This indicates that thermo-optic effect, i.e., coupling between phonon gas and light, which is negligible in gases and liquids, can be strong in ferroelectrics or "incipient" ferroelectrics such as rutile or $SrTiO_3$. Semiconductors with absorption edge in visible wavelength region have also relatively large $(\partial n/\partial T)_u$ probably because of the temperature dependence of energy band gap. ZnSe is an orange-colored semiconductor with absorption edge of 480 nm at 300 K.[39] The refractive index and its temperature coefficient for a nearly resonant excitation light source are larger than those in transparent region. Although the values of $(\partial n/\partial T)_u$ for the employed wavelengths $\lambda=514.5$ and 476.5 nm are not available, it has been reported that $(\partial n/\partial T)_u$ for $\lambda<632.8$ nm can be larger than $+10^{-4}$/K,[42] which is as large an absolute value as that of $(\partial n/\partial T)_u$ in rutile. Note that liquids also have large dn/dT, but it is largely due to thermal expansion. Further-

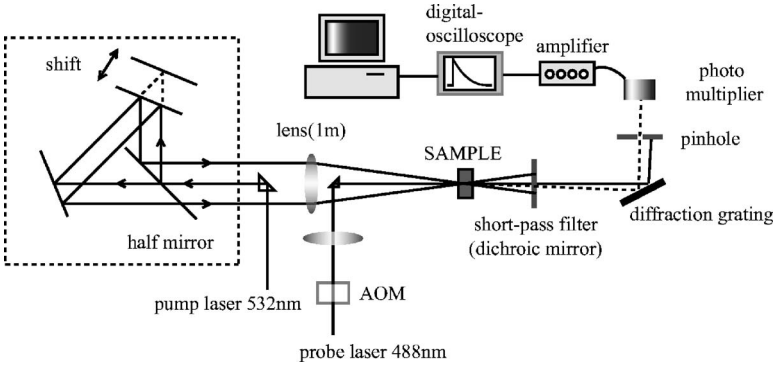

FIG. 2. Experimental setup for ISTS. Here, AOM represents acousto-optic modulator. The modified Sagnac interferometer, which is enclosed with the dashed lines, enables continuous change of beam separation without causing any time delay between the two separated pulses at the focused position.

more, the liquids' $(\partial n/\partial \rho)_T$ is much larger than $(\partial n/\partial T)_\rho$, where we have replaced strain u with density ρ.

The samples of rutile, ZnSe, and $SrTiO_3$ were bulk crystals, while that of silicon was a wafer with a thickness of 1 mm. The scattering angle was $180 \pm 9.4^\circ$, and the values of q were estimated to be 7.3×10^7, 7.5×10^7, 10.2×10^7, 6.0×10^7 m^{-1} in rutile, ZnSe, silicon, and $SrTiO_3$, respectively. The directions of $\boldsymbol{q}$ in the sample crystals were rather roughly chosen, and they were approximately in the directions of crystalline [100], [110], [111], and [001] for rutile, ZnSe, silicon, and $SrTiO_3$, respectively. However, slightly different directions were occasionally adopted when the samples were slightly tilted for reduction of parasitic elastic scattering intensity from the surface of the samples. The wavelength of the light source (Ar^+ laser) was 514.5 nm for rutile, silicon, and $SrTiO_3$, and 476.5 and 514.5 nm for ZnSe. The samples were placed either in a flow-type cryostat or in a oven, and the temperature was changed from 4.2 to 673 K for rutile, from 200 to 600 K for silicon, and from 4.2 to 300 K for ZnSe and $SrTiO_3$.

B. Impulsive stimulated thermal scattering (ISTS)

1. Principle of measurement

Although it is hard to obtain a small q value in ordinary light scattering experiments, it can be fairly easily realized in the well-established technique of ISTS.[20,21] In ISTS, the fringes formed by the two intersecting pulsed pump beams heats up the sample locally, and then the provided heat diffuses to realize thermal equilibrium. Since the "hot fringes" act as a diffraction grating with a pitch of $2\pi/q$, with another probing continuous-wave (cw) light beam incident into the sample, the temporal evolution of the transient grating can be observed in real time by monitoring the Brag-diffracted intensity of the probe cw beam. If the pulse width is broader than $2\pi/\omega_B$, the Brillouin component cannot be resolved, and the diffracted light intensity has a time dependence as[20]

$$I_{\text{probe}} = A\exp(-2\Gamma t) + B, \tag{10}$$

where A and B are constants and Γ is the relaxation rate. The factor 2 in the exponent appears because $I_{\text{probe}} \propto |E_{\text{probe}}|^2$, where the probe field E_{probe} decays as $\exp(-\Gamma t)$. For the hydrodynamic phonon regime, Γ corresponds to the rate of thermal diffusion, i.e., $\Gamma = D_{\text{th}} q^2$. In the ISTS, Eq. (2) can be approximated as

$$q = \frac{2\pi}{\lambda}\theta, \tag{11}$$

where θ is now the intersecting angle of the two pump beams measured outside the sample. Note that the refractive index n is not present in Eq. (11) in contrast to Eq. (2) because of cancellation of n due to Snell's law at the sample boundary. For visible light with $2\pi/\lambda \approx 10^7$ m^{-1}, the value of q can be reduced to less than 10^5 m^{-1} by setting θ to $\lesssim 10$ mrad, which is easily achieved in the ISTS configuration by focusing the two parallel pump beams, which are separated by $\lesssim 1$ cm, at a distance of $\gtrsim 1$ m.

2. Experimental setup for ISTS

The experimental setup for the ISTS is depicted in Fig. 2. The pump laser was the second harmonic of a pulsed Nd:yttrium-aluminum-garnet (YAG) laser, and the wavelength was 532 nm. Since all the samples investigated except Si are transparent around 530 nm, the thermal grating is considered to be generated by two-photon absorption of the two intersecting light pulses. The pulse width and the repetition rate were 8 ns and 10 Hz, respectively. The pump beam was split by a beam splitter and each of the split beams was reflected twice by two mirrors, one of which was spatially shifted by an X stage to change the separation between the two pump beams at the position of the focusing lens. Note that in this modified Sagnac interferometer the two split light pulses are always synchronized at the position of the focusing lens because the path lengths are the same for the two paths. The intersecting angle of the two pump beams was varied by changing either the beam separation at the position of the focusing lens or the focal length of the lens. The probe laser was a cw Ar^+ laser oscillating in a single longitudinal mode at 488 nm. To prevent samples from heating by the probe beam, an acousto-optic modulator (AOM) was inserted into the probe beam path to reduce its duty. The probe beam was focused into the sample by a 1 m focal lens. After filtering the pump light by a short-wave-pass dichroic mirror and a diffraction grating, the signal light was detected by a photomultiplier tube and the amplified signal was monitored by a digital oscilloscope (300 MHz) and recorded by a computer after 30 time averages. We did not investigate the silicon sample by ISTS not only because silicon is opaque for the above light sources, but also because the sample of silicon was a wafer with a thickness of 1 mm, which was difficult to measure by the present ISTS apparatus. The values of

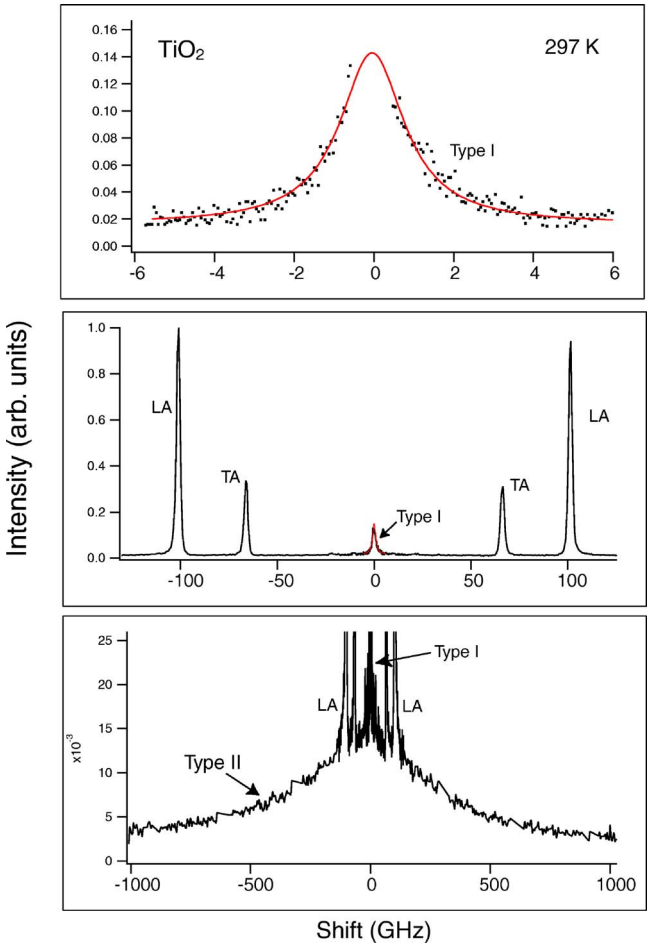

FIG. 3. (Color online) Backscattered spectrum observed in rutile at 297 K with $\boldsymbol{q}\|[100]$. The LAs and TAs represent longitudinal and transverse acoustic Brillouin lines, respectively. The two QELS components are labeled as types I and II. The smooth curve is a Lorentzian fit to the QELS I. Note that the vertical scales are normalized at the peak height of the LA Brillouin component. Also note that the middle and the lower spectra are constructed by combining the spectra obtained at different resolutions.

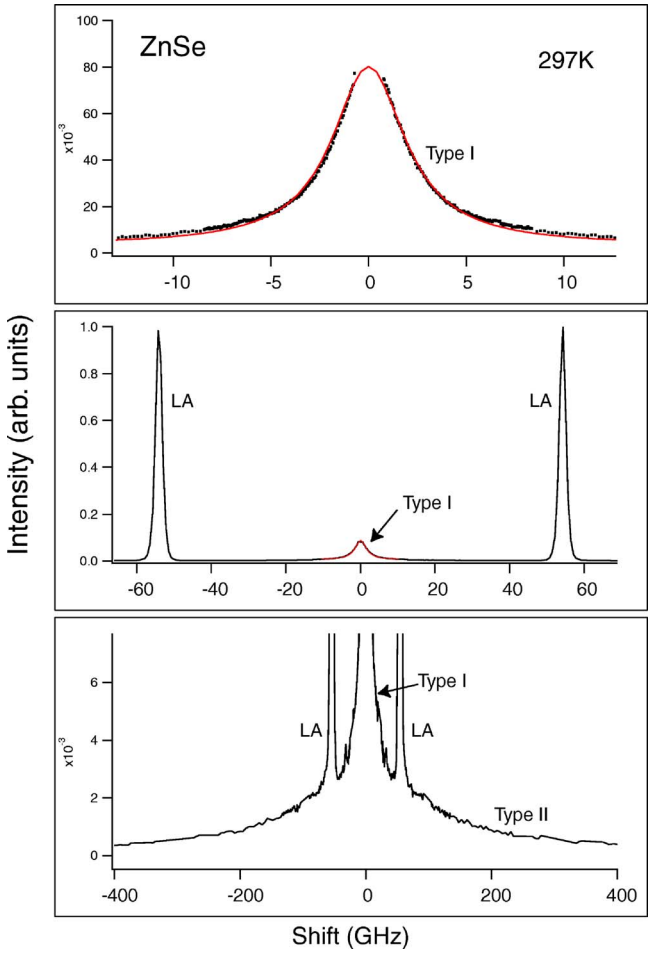

FIG. 4. (Color online) Backscattered spectrum observed in ZnSe at 297 K with $\boldsymbol{q}\|[110]$. The LAs and TAs represent longitudinal and transverse acoustic Brillouin lines, respectively. The two QELS components are labeled as types I and II. The smooth curve is a Lorentzian fit to the type I QELS. Note that the vertical scales are normalized at the peak height of the LA Brillouin component. Also note that the middle and the lower spectra are constructed by combining the spectra obtained at different resolutions.

q employed for all the investigated samples were 1.54×10^5, 1.37×10^5, 1.08×10^5, 9.12×10^4, and 8.07×10^4 m^{-1}, which were estimated from Eq. (11) from the measured θ's (the beam separations divided by the focal length). Again, the directions of $\boldsymbol{q}$ in the crystals were rather roughly chosen, and they are almost the same as those employed in the backscattering experiments described in Sec. III A.

IV. EXPERIMENTAL RESULTS

A. Results for backscattering

The backscattering spectra obtained in rutile, ZnSe, silicon, and $SrTiO_3$ are shown in Figs. 3–6, respectively. All the spectra presented here were recorded with parallel incident and scattered light polarizations, i.e., with either *VV* or *HH* configurations, where *V* and *H* represent vertical and horizontal polarizations, respectively. We will refer to the narrower component as "type I" and to the broader one as "type II" as labeled in the figures. Note that the elastically scattered peaks are removed from all the spectra. We see that the QELS I does not extend beyond the longitudinal acoustic (LA) Brillouin peaks, whereas the QELS II spreads out to the Brillouin lines and usually couples to them, resulting in the asymmetric line shapes for the Brillouin component as can be seen in Figs. 3, 4, and 6. In the spectra of silicon, we cannot clearly resolve the QELS II and separate it from type I for two reasons. First, the QELS II is far weaker than the QELS I. Second, the linewidth of the QELS I is not sufficiently narrow compared to that of the weak QELS II, making it difficult to distinguish the QELS II from the spectral tail of type I. However, the linewidth of the QELS II, which we have obtained at room temperature, is in good agreement with that reported by Stoddart and Comins,[16] where the QELS II was recorded more clearly and the asymmetry of the LA Brillouin lines was also clear. Nevertheless, we cannot give an accurate temperature dependence of the QELS II in silicon because of the insufficient signal-to-noise ratio. A

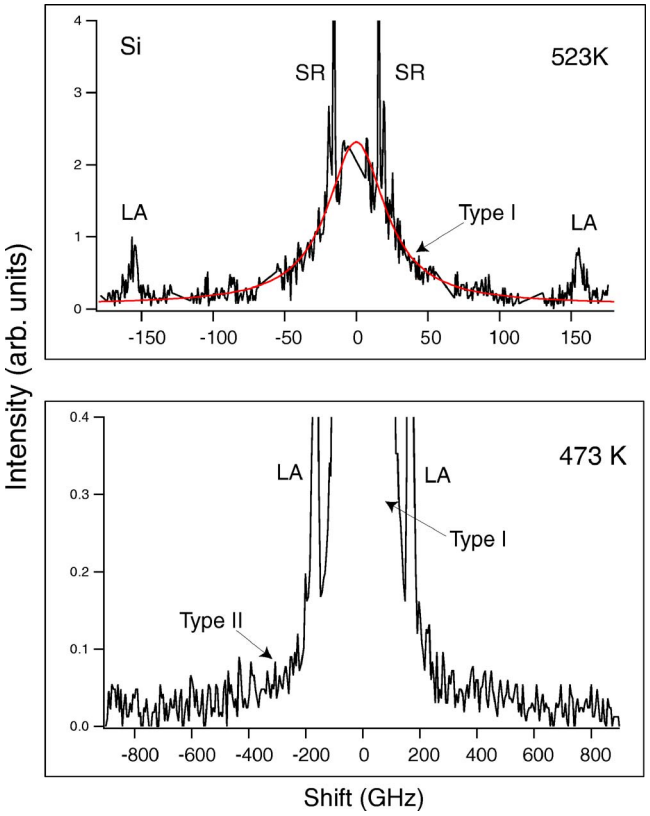

FIG. 5. (Color online) Backscattered spectrum observed in silicon at comparable temperatures of 523 K (upper) and 473 K (lower) with $\boldsymbol{q}\|[111]$. The LAs and SRs represent the Brillouin scattering due to longitudinal acoustic and surface Rayleigh modes, respectively. The two QELS components are labeled as types I and II. The smooth curve is a Lorentzian fit to the type-I QELS. Note that the vertical scales are normalized at the peak height of the LA Brillouin component. In the lower trace, the QELS II is very weak and cannot be well separated from the components of the type I and the Brillouin.

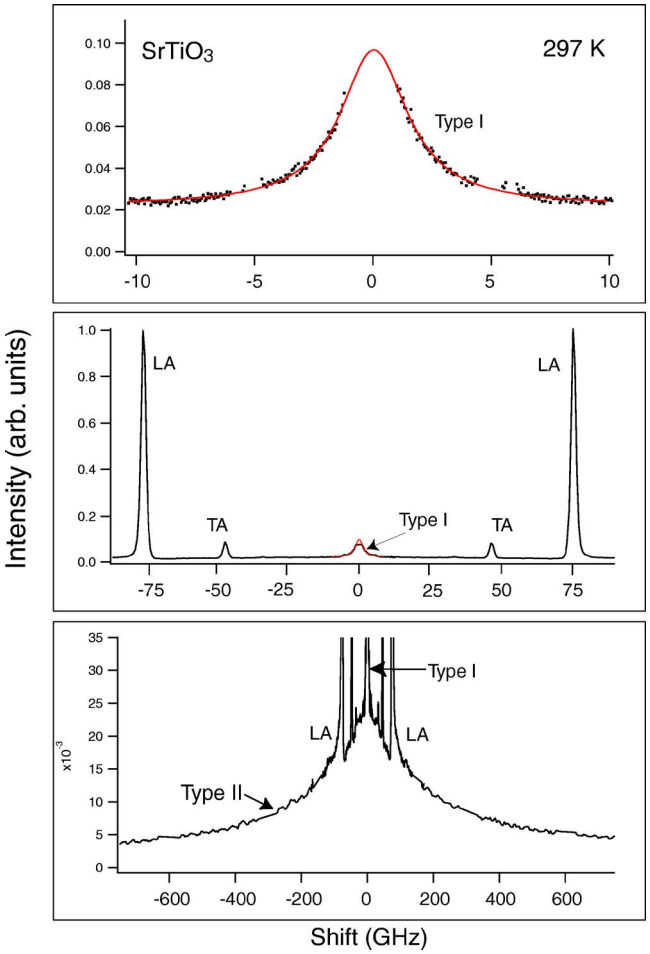

FIG. 6. (Color online) Backscattered spectrum observed in $SrTiO_3$ 297 K with $\boldsymbol{q}\|[001]$. The LAs and TAs represent longitudinal and transverse acoustic Brillouin lines, respectively. The two QELS components are labeled as type I and II. The smooth curve is a Lorentzian fit to the type-I QELS. Note that the vertical scales are normalized at the peak height of the LA Brillouin component. Also note that the middle and the lower spectra are constructed by combining the spectra obtained at different resolutions.

wider free spectral range of the interferometer might give better resolution as a trade-off with signal to noise ratio.

For the QELS I, the spectra have been successfully fitted by Lorentzians with appropriate constant backgrounds, which reasonably approximate the much wider QELS II in the relevant frequency range for the type-I spectra. The fitted curves are also presented in Figs. 3–6. Although the type-II QELS has no necessity to become a Lorentzian,[14–16] it has been also well fitted by Lorentzians in rutile, ZnSe, and $SrTiO_3$ by removing the Brillouin lines and the QELS I from the spectra when performing least-squares fit. In silicon, however, the scattering intensity was so weak that either Lorentzian or Gaussian could be poorly fitted to the QELS II. In other samples, decomposition into the two types of QELS was easier at relatively high temperatures because the two QELS exhibit opposite temperature dependence and the difference in their linewidth is larger at higher temperatures as we will see later in this section. At relatively low temperatures, however, we had to fit a double unshifted Lorentzian to the composite of the two QELS. We will describe our fitting procedure in more detail later in this section.

This kind of two-component QELS has been observed in several materials such as $KTaO_3$,[12] diamond,[14] and silicon.[4,13,16] However, detailed temperature dependences of the intensity and the linewidth for both types of QELS have been investigated only recently for rutile,[15] and a unified explanation for both components in terms of two-phonon difference Raman processes has also been suggested. The QELS I has been ascribed to entropy fluctuations in the hydrodynamic phonon regime, while in the collisionless regime this component must be considered as arising due to two-phonon difference Raman processes, in which two phonons on a single phonon branch participate.[14,15] On the other hand, the QELS II has been ascribed to two-phonon difference Raman processes, in which two phonons on *different* phonon branches participate.[15] In general, the width of the QELS II has little q dependence, and almost linearly decreases with decreasing temperature as reported long ago in $KTaO_3$,[12] diamond,[14] and recently in rutile.[15] While the QELS II has been explained qualitatively by two phonon difference scattering,

any quantitative explanation has not been given so far except for the temperature dependence of the integrated intensity in rutile,[15] and room for more detailed study has been still left for the origin of this component. It can be considered that both types of QELS arise from phonon-density fluctuations in the sense that the number of phonons is changed via lattice anharmonicity in both kinds of light scattering processes.[5] It may be noted that the unified explanation for the two component QELS in terms of the simple two-phonon difference light scattering model implies that QELS due to phonon-density fluctuations in dielectric crystals should essentially consist of two components, namely, QELS I and II in our terminology. In the remaining part of this paper, however, we will refer inlarge part to the linewidth of the QELS I because the linewidth of the QELS II does not exhibit q-dependence and also because it has too high frequency ($\sim$ THz) to investigate by our ISTS apparatus.

For rutile, we have investigated the temperature variation of the spectra in a wider temperature range, i.e., from 20 to 600 K, than that presented in Ref. 15 because the Debye temperature of rutile is relatively high[43] (760 K) and we consider that it is important to investigate the higher temperature region in order to characterize the phonon regime in this material.

For ZnSe, an interesting resonance light scattering effect[34] has been observed at 297 K when the wavelength of the excitation light was 476.5 nm, which was close to the absorption edge of ZnSe at room temperature.[39] The resonance effect greatly enhanced the scattering intensity not only for the LA Brillouin lines[44–46] but also for the both types of QELS component. However, we could not find differences in both line shapes and linewidths of all the scattering components within the experimental error when the different excitation wavelengths were employed. We have also observed in the ZnSe sample a luminescence around the excitation wavelength of 514.5 nm at temperatures lower than approximately 100 K. The intensity of the luminescence was comparable to or stronger than the QELS II at lower temperatures, and it gave rise to slanted background in the spectra. However, the origin of this luminescence is not yet clear so far and the discussion regarding this will not be included in this paper. Although we were able to see the QELS II in ZnSe at temperatures as low as 100 K, we analyzed it only for 150, 200, and 297 K because of its weak intensity, the relatively strong luminescence, and the linewidth not wide enough to be separated from the QELS I at low temperatures. The spectrum in Fig. 4 was obtained with excitation wavelength of 514.5 nm.

The temperature dependences of the linewidth of the QELS I and II, to which we refer as Γ_I and Γ_{II}, respectively, are shown in Fig. 7. Note that the ordinate axes are measured in units of angular frequency (rad/s) rather than in units of frequency ($\Gamma/2\pi$). The plotted points represent the measured linewidths (half width at half maximum) and the curves are the values derived from macroscopic theory, viz., $D_{\text{th}}q^2$. The values for D_{th} were obtained from the relation $D_{\text{th}}=\kappa/(\rho C)$, where κ, ρ, and C are the thermal conductivity, the mass density, and the specific heat, respectively, which were available in the literatures.[32,33,39,47–49] We have extrapolated the unavailable values for D_{th} for rutile at temperatures above 400 K, taking into account that $D_{\text{th}} \propto T^{-1}$ at high temperatures because of Eq. (3).

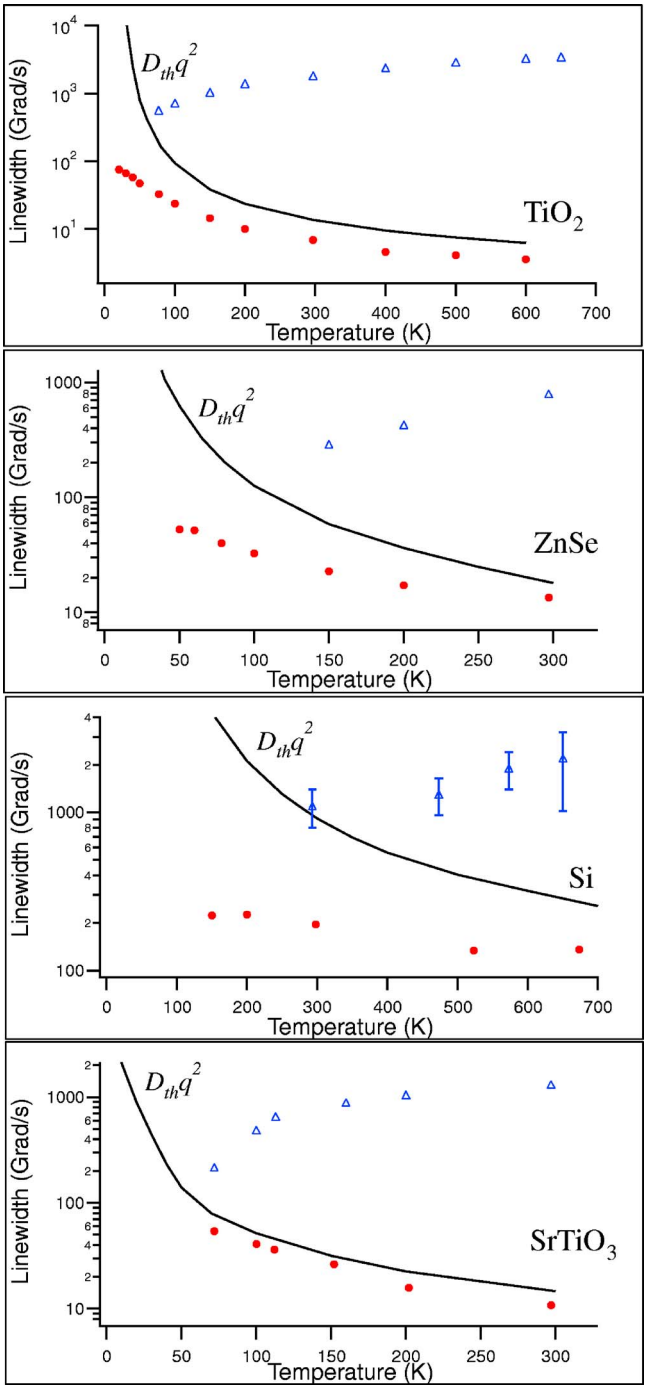

FIG. 7. (Color online) The temperature dependence of the linewidth for the type I and II QELS's measured by backscattering in TiO_2 (rutile) ($q=7.34\times10^7$ m^{-1}), ZnSe ($q=7.49\times10^7$ m^{-1}), silicon ($q=10.2\times10^7$ m^{-1}), and $SrTiO_3$ ($q=6.00\times10^7$ m^{-1}). The circles and the triangles represent Γ_I and Γ_{II}, respectively. The solid curves represent the $D_{\text{th}}q^2$ values. Note that the ordinate axes is scaled logarithmically and the unit is in angular frequency rather than in units of frequency ($\Gamma/2\pi$).

In Fig. 7, the measured Γ_I's are considerably narrower than $D_{\text{th}}q^2$ at relatively low temperatures except for $SrTiO_3$. The values of the phonon Knudsen number at the lowest temperatures in rutile, ZnSe, and silicon are estimated to be 78, 22, and 20, respectively, while that in $SrTiO_3$ to be 0.81.

Thus, it is considered that this large difference between the measured Γ_I and $D_{th}q^2$ for rutile, ZnSe, and silicon is due to the fact that the phonon Knudsen number $q\bar{l}$ is larger than unity in these low temperature regions, and the macroscopic quantities cannot be defined locally.[13–15,17] On the other hand, in $SrTiO_3$, the small value of $q\bar{l}$ implies that phonon collisions are still frequent at temperatures as low as 70 K.

The linewidths of the QELS II, Γ_{II}, is also plotted as open triangles. In contrast to Γ_I, Γ_{II} was almost independent of q values, and nearly linearly decreases with decreasing temperature (when plotted with linear ordinate axis) as reported earlier.[12,15] In silicon, however, we could not investigate the q dependence of Γ_{II}. Although there is no report on the clear q dependence of the broader QELS in silicon, the asymmetric Brillouin line shape reported by Stoddart and Comins[16] is likely evidence that this broader component in silicon can be identified as QELS II.

The linewidths of the QELS I presented in Fig. 7 have been obtained basically by least-squares fit of a Lorentzian in the frequency ranges for the type-I QELS, with the intensity of the much broader QELS II as a constant background. Γ_{II} has been obtained by excluding the Brillouin lines and the QELS I in the fit. However, in some low-temperature regions, Γ_{II} may narrow to become only several times broader than Γ_I. In this case, it was hard to fit a single Lorentzian in the type-I frequency region, so we have fitted unshifted double Lorentzians with different linewidths and intensities for such spectra: appropriate initial values for the fitting parameters have given a reasonable result taking into account the temperature dependences of both Γ_I and Γ_{II}. At even lower temperatures where the two linewidths would coincide, we found that only either type-I or -II QELS was actually visible: only type I was visible in rutile, ZnSe, and silicon, while only the QELS II in $SrTiO_3$. In practice, the least-squares fit succeeded if the linewidths were different by more than a factor of 10. However, the spectra at 100 K or below in ZnSe could not be reasonably fitted even with the double unshifted Lorentzians because the linewidths and the intensities of the two QELS components were too close to each other. The values of Γ_{II} for silicon contain large uncertainties, which are shown as error bars in Fig. 7, not only because of its weak scattering intensity and low signal to noise ratio in our experiment but also because of the existence of the relatively broad and intense type-I QELS and Brillouin components, which obscure the accurate line shape of the QELS II.[16] In fact, Γ_{II} could not be obtained by least-squares fit and was read directly from the spectra with removing and interpolating the frequency range for the QELS I and the Brillouin lines. Nevertheless, our value of Γ_{II} in silicon at 300 K is in good agreement with that reported by Stoddart and Comins[16] at room temperature: the reported "300- to 400-GHz full width" in units of frequency gives 940 to 1300 Grad/s half width in units of angular frequency, which enters in the same range as our value. Note that Γ_{II} in silicon at 300 K is accidentally close to $D_{th}q^2$, which might cause misidentification of the QELS II as an EFLS.

For $SrTiO_3$, the two component QELS was reported about thirty years ago,[12] but detailed spectral variation of the type-I QELS (EFLS) in a wide range of temperature has not yet been reported to the best of our knowledge. We show in Fig. 8 the spectral variation of the QELS I in $SrTiO_3$ in the temperature range from 72 to 297 K. Except the temperature of 72 K, a single Lorentzian with a constant background has been successfully fitted to the QELS I, while for 72 K a double unshifted Lorentzian with different widths has been assumed and fitted because the QELS II was not broad enough to be regarded as a flat baseline at this temperature. It should be noted that in Fig. 7 the measured Γ_I in $SrTiO_3$ is almost equal to $D_{th}q^2$ at all temperatures investigated ($\gtrsim$72 K), indicating that the phonon density is much higher in this material than in others investigated. The well-known structural phase transition in $SrTiO_3$ at 105 K exhibited little divergent behavior on the linewidths of both types of QELS within the experimental error as reported earlier,[3] while the Brillouin linewidth considerably increased and the total scattering intensity, including the Brillouin lines and the two QELS components, slightly increased around 105 K. This slightly divergent behavior of Γ_I is consistent with the temperature dependences of the thermal conductivity[50] and the specific heat,[48,49] whose reported relative changes accompanied by the phase transition at 105 K is as small as 2%, which is too small to be distinguished in the present apparatus. However, a more careful investigation of Γ_I around 105 K in $SrTiO_3$ may reveal a relatively small but steep changes in the thermal diffusivity as one can expect from the detailed temperature dependences of the specific heat[49] and the elastic constants.[51]

In $SrTiO_3$ at lower temperatures, where the QELS I was not visible, however, a broad doublet spectrum as shown in

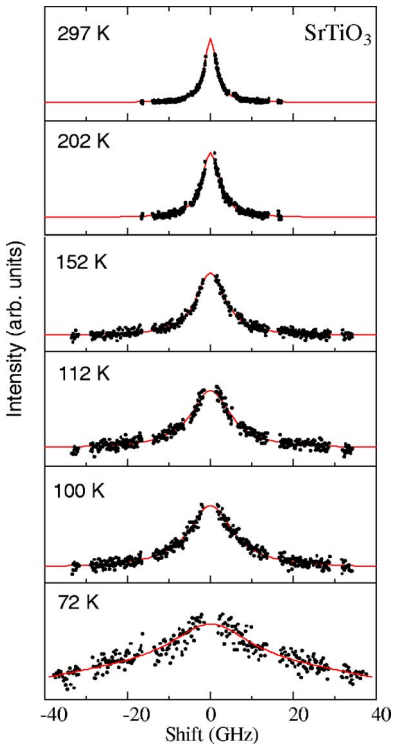

FIG. 8. (Color online) Temperature variation of the type-I QELS in $SrTiO_3$. The dots are the experimental spectra and the smooth curves are least-squares fits. For 72 K, a double unshifted Lorentzian has been assumed and fitted.

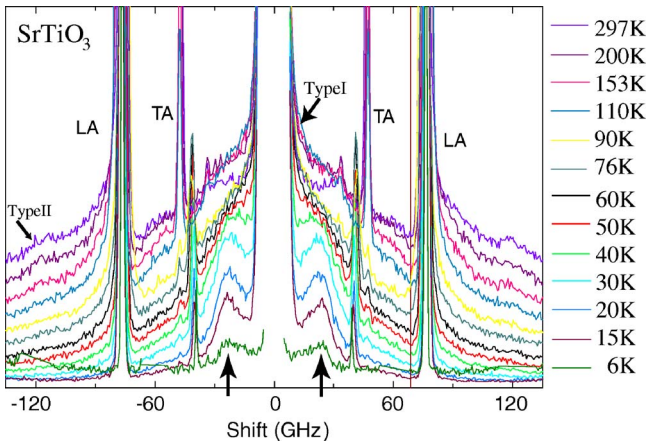

FIG. 9. (Color online) The broad doublet spectra observed in $SrTiO_3$: from the upper trace, 297, 200, 153, 110, 90, 76, 60, 50, 40, 30, and 15 K. The arrows indicate the broad doublet, and the LA's and TA's represent longitudinal and transverse acoustic Brillouin lines, respectively. The direction of $\boldsymbol{q}$ was chosen to be almost parallel to crystalline [100] direction in cubic symmetry. The TA Brillouin frequency changes across the structural phase transition temperature of 105 K.

Fig. 9 has been found. This was first observed by Hehlen *et al.*,[9] in an oriented (single domain) sample of $SrTiO_3$ and has been tentatively explained as arising due to second sound,[9,52–54] or more recently reproposed to be due to two-phonon difference scattering,[55] but the origin for this component is still controversial. In our experiment, the direction of $\boldsymbol{q}$ was chosen to be almost parallel to crystalline [100] direction of cubic symmetry, and the signal was observed in the same polarization direction of the incident light. Not as the previous report,[9] our sample seems to have multiple domains below 105 K since we have not applied any uniaxial pressure to orient the domains in the same direction. Thus, the direction of $\boldsymbol{q}$ in the tetragonal symmetry could not be determined explicitly. The frequency shift and the linewidth of the doublet was in good agreement with that reported by Hehlen *et al.*[9]

B. ISTS results

The temporal profiles measured in the ISTS are similar in all the samples investigated, namely, rutile, ZnSe, and $SrTiO_3$. Typical ISTS signals measured in the sample of rutile at various temperatures are shown in Fig. 10 as an example. The traces in the left half of Fig. 10 are displayed from 0 to 100 μs, while those in the right half are from 0 to 5 μs. As the temperature is lowered, the exponential decay becomes faster because the thermal diffusivity increases with decreasing temperature.

In addition to the signal due to thermal diffusion, there is a much faster component superposed on the thermal diffusion profile at relatively high temperatures in all the samples investigated: in rutile, for example, it is seen in Fig. 10 at temperatures 296 and 202 K. We consider this fast component as arising from third order nonlinear susceptibility for

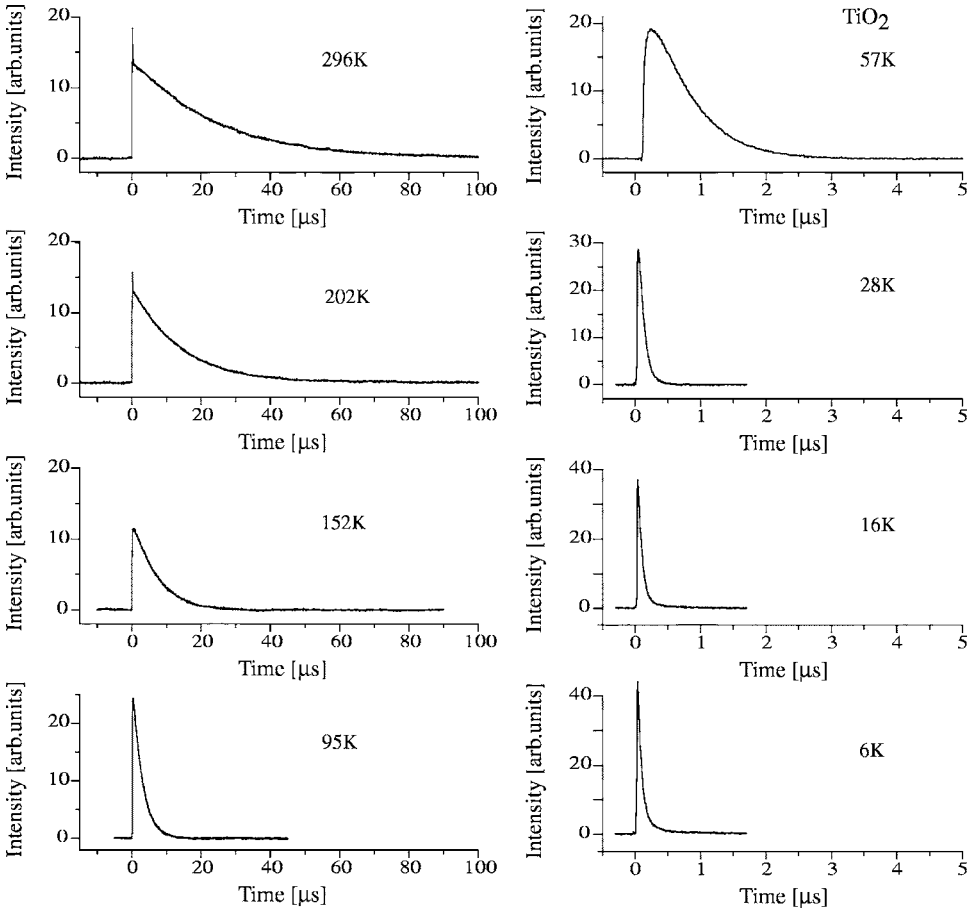

FIG. 10. Temperature dependence of the ISTS signal in TiO_2 (rutile) in the temperature range from 6 to 296 K. The left graphs are traced from 0 to 100 μs, while the right ones are traced from 0 to 5 μs. The origin of the spikes appearing at temperatures 296 and 202 K is discussed in the text.

ZnSe, and as arising from spatial distribution of excitons, which are excited via two-photon absorption of the pump light, for rutile and $SrTiO_3$. Furthermore, in $SrTiO_3$, there is another component which decays much more slowly than the thermal diffusion signal. We consider this slower component in $SrTiO_3$ to be due to relaxation from an energy level located between the valence and conduction bands, so called "midgap level," whose lifetime is known to be very long.[56] Although these additional components are of interest, they are out of the main subject of this article, and we will not refer to them hereafter.

The temperature dependence of Γ_I obtained by ISTS is shown in Fig. 11 for rutile, ZnSe, and $SrTiO_3$ with normalized by q^2. Note that Γ_I/q^2 is expected to be equal to D_{th} in the hydrodynamic regime. The solid curves are interpolations of the D_{th} values obtained from the literatures.[32,33,39,47] In contrast to the results for backscattering shown in Fig. 7, the measured values of Γ_I/q^2 now follow the D_{th} curves even at fairly low temperatures for all the three materials investigated. These results indicate that the probe light is scattered by a gas of phonons and the macroscopic heat-transport theory actually remains valid even at low temperatures, namely, $\gtrsim$50 K for rutile and ZnSe, and $\gtrsim$15 K for $SrTiO_3$. Below these temperatures, however, the measured values of Γ_I/q^2 begin to deviate from D_{th} curves on cooling just as we have seen in the backscattering experiments, probably indicating that the macroscopic theory is no longer valid at such low temperatures also in the ISTS. We will discuss on this point later in Sec. V B.

For $SrTiO_3$, it is very interesting to point out that the measured Γ_I/q^2 values are well reproduced by D_{th} at all the temperatures investigated except the lowest 6 K. The suggested possibility for the existence of second sound in $SrTiO_3$ below 40 K (Refs. 9 and 52–54) is closely related to the phonon Knudsen number through the well-known "window condition."[57] It is known that the energy of the transverse optical phonon modes in $SrTiO_3$ are anomalously low[53] and, therefore, there should be many phonons excited even at low temperatures.[52] In fact, both the ISTS and the back-scattering results clearly indicate that there are exceptionally many phonons (or more rigorously, many phonon collisions) even at low temperatures in $SrTiO_3$. This is a very interesting fact in connection with the possible existence of second sound in $SrTiO_3$. We will present more detailed discussions on the results in $SrTiO_3$ in Sec. V A.

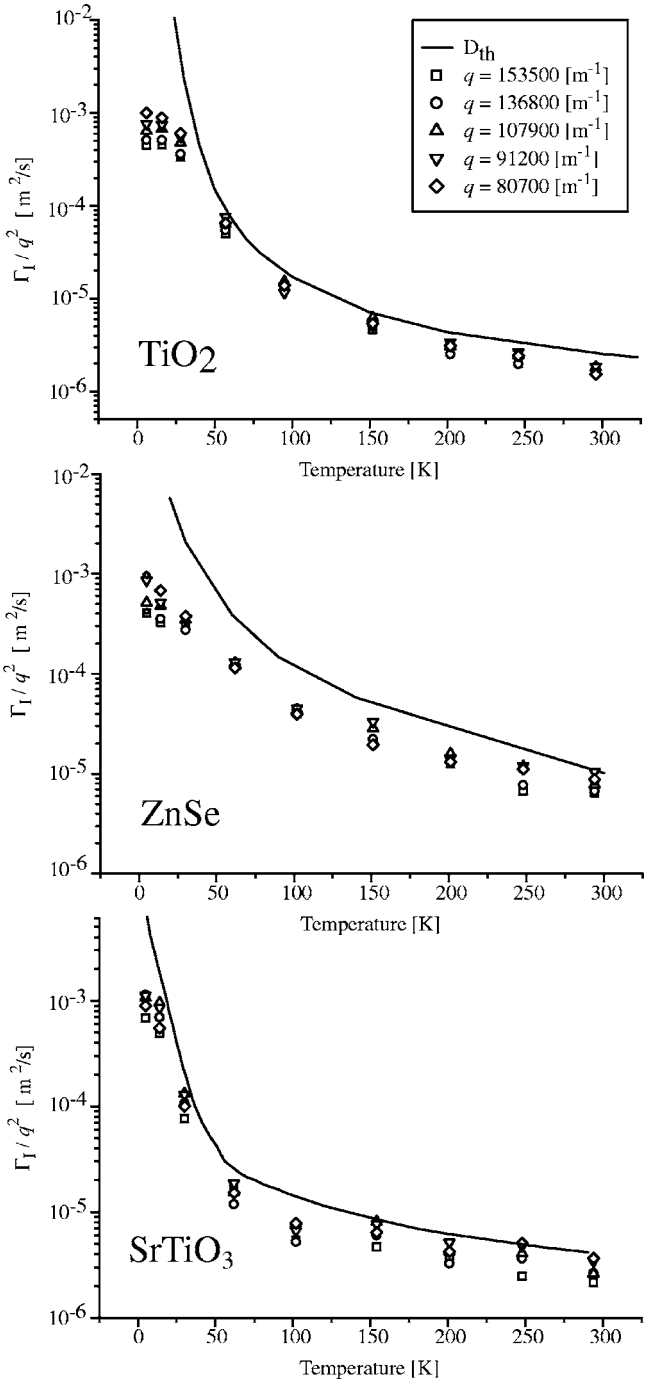

FIG. 11. Temperature dependence of Γ_I measured by ISTS in TiO_2 (rutile), ZnSe, and $SrTiO_3$. The ordinate axes are logarithmically scaled and normalized by q^2 for direct comparison with D_{th}. The values of q are indicated in the inset. The measured values well follow the D_{th} curves in a wide range of temperature.

V. DISCUSSIONS

We have shown in Sec. IV the experimental results of the temperature dependence of Γ_I for various magnitudes of q. Now we consider to unify the data presented so far, by plotting the measured Γ_I against the phonon Knudsen number $q\bar{l}$. We use the same literature values for D_{th} as those employed in the earlier part of this article in the estimation of $\bar{l}$. In terms of $\bar{v}$ in Eq. (3), we define an average Brillouin frequency as follows:

$$\bar{\omega}_B = q\bar{v}. \tag{12}$$

Note that we neglect any anisotropy of crystal lattices and variations of phonon-collision type[58,59] for simplicity in the discussions made here. We also define γ_I as a type-I linewidth normalized by the average Brillouin frequency $\bar{\omega}_B$, i.e.,

$$\gamma_I = \frac{\Gamma_I}{\bar{\omega}_B}.$$

Similarly, we define the normalized linewidth for Γ_{II} measured by backscattering as

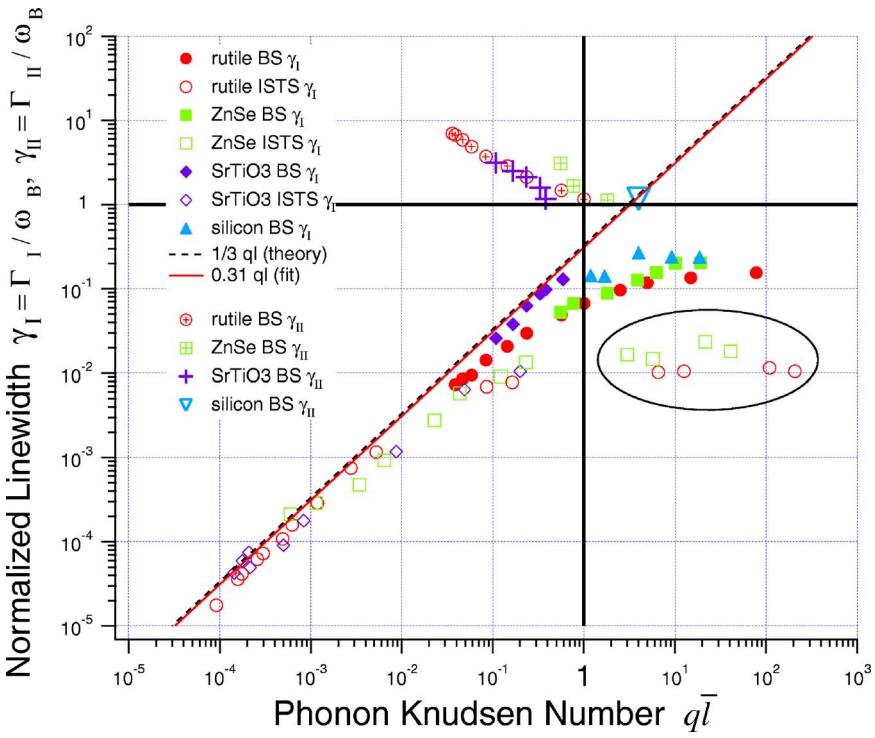

FIG. 12. (Color online) The linewidths of the QELS I and II in the units of the average Brillouin frequency versus the phonon Knudsen number $q\bar{l}$. Legends for the symbols are shown in the figure. The ISTS data points circled by the oval are considered as artifacts, and they should be shifted to $q\bar{l} \lesssim 1$ according to the discussion made in the text. For Γ_{II} in silicon, only the room temperature value is presented here because of the lack of accuracy for other temperatures.

$$\gamma_{II} = \frac{\Gamma_{II}}{\omega_B}.$$

Figure 12 is a plot of γ_I and γ_{II} against the phonon Knudsen number $q\bar{l}$. For the ISTS data, we have plotted only the measured points for $q = 80\,700$ and $153\,500\ \mathrm{m}^{-1}$, which are, respectively, the smallest and the largest values of q employed in our ISTS experiments. For Γ_{II} in silicon, only the room temperature value is presented here because of the large uncertainties at other temperatures. It is surprising that all the normalized linewidth of QELS I measured in different materials seem to coincide in a certain function of phonon Knudsen number. In addition, we see that γ_{II} has a $(q\bar{l})^{-1}$ dependence and $\gamma_{II} \gtrsim 1$ in rutile, ZnSe, and $SrTiO_3$.

In the following part of this section, we discuss on the three types of phonon regime, namely, the hydrodynamic, the collisionless, and the intermediate regimes, in detail with reference to Fig. 12. Also an empirical function that can be fitted to the measured γ_I as a function of $q\bar{l}$ is introduced and discussed. We also present a brief discussion on γ_{II} concerning its magnitude and dependence on the phonon Knudsen number $q\bar{l}$.

A. The hydrodynamic regime—the entropy-fluctuation light scattering

In Fig. 12, the hydrodynamic phonon regime corresponds to the region such that $q\bar{l} \ll 1$. We find that γ_I in the hydrodynamic phonon regime is proportional to the phonon Knudsen number $q\bar{l}$ because the slope is approximately 1 in the log-log plot. In fact, a simple linear function such as

$$\gamma_I \simeq 0.31 q\bar{l} \tag{13}$$

was successfully fitted to the region $q\bar{l} < 0.001$. This is in good agreement with what is expected for the EFLS with a well-known q^2 dependence for its linewidth, i.e.,

$$\Gamma_I = D_{\mathrm{th}} q^2 = \frac{1}{3} \bar{\omega}_B q\bar{l}, \tag{14}$$

where we have used Eqs. (3) and (12). Equations (13) and (14) are shown in Fig. 12 as solid and dashed lines, respectively, which almost coincide with each other.

Furthermore, we find in Fig. 12 that γ_I is substantially smaller than unity, i.e., $\Gamma_I \ll \bar{\omega}_B$, in the hydrodynamic regime. Therefore, we may say that the linewidth of an EFLS *must* be sufficiently smaller than the Brillouin frequency. In fact, in the hydrodynamic phonon regime, since $q\bar{l} \ll 1$,

$$\frac{\Gamma_{\mathrm{EFLS}}}{\omega_B} = \frac{1}{3} \frac{\bar{v}}{v_B} q\bar{l} \ll 1.$$

This equivalently means that a QELS, whose linewidth is not sufficiently narrower than the Brillouin frequency or extends out of the LA-Brillouin peaks, is *not* an EFLS even if its linewidth is close to $D_{\mathrm{th}} q^2$ because of the violation of local thermal equilibrium. For example, as can be seen in Fig. 7, the QELS observed in silicon with a linewidth $\approx D_{\mathrm{th}} q^2$ at room temperature was first identified as EFLS,[60] but it has been later reassigned to QELS II instead of EFLS (Ref. 16) since the spectrum *did* extend out of the LA-Brillouin peaks. In the frequency region higher than ω_B, entropy fluctuation or other thermodynamic quantities cannot contribute to light scattering because local thermal equilibrium is not achieved so fast, and such macroscopic quantities can no longer be considered. In stead, we have to consider some kinetic scattering models such as second order light scattering for such fast processes.[5,7,8,13,15]

B. The collisionless regime

In the collisionless regime, i.e., when $q\bar{l} \gg 1$, γ_{I} tends to become constant, viz., ~0.2 or ~0.02, with increasing phonon Knudsen number as shown in Fig. 12. The two different limiting values, i.e., ~0.2 and ~0.02, correspond to the results obtained by the backscattering and the ISTS experiments, respectively. However, we consider the latter value as an artifact due to overestimation of $\bar{l}$ in plotting the ISTS data in Fig. 12.

In the ISTS, a thermal grating, or more rigorously, a "phonon-density grating" is generated by the two pump electric fields: the initial phonon density is high along the ridges of the grating, which are periodically spaced with a spatial period of $2\pi/q_{\mathrm{ISTS}}$, where q_{ISTS} is the magnitude of wavevector transfer in ISTS. If the temperature is sufficiently high such that $\bar{l} \ll 2\pi/q_{\mathrm{ISTS}}$, then ISTS can give a correct thermal diffusivity. However, we consider that $\bar{l}$ does not exceed $\simeq 2\pi/q_{\mathrm{ISTS}}$ or $\simeq 1/q_{\mathrm{ISTS}}$ in the ISTS because a phonon distribution with a spatial period of $2\pi/q_{\mathrm{ISTS}}$ is always generated forcibly by the pump laser. In other words, even if the phonon density outside the generated grating is very low, a phonon inside a grating ridge always has neighbor phonons to collide with within a distance of $2\pi/q_{\mathrm{ISTS}}$. This means that the MFP of phonons in the ISTS cannot be longer than the generated grating pitch. Thus, the longest MFP of phonons possible in the ISTS should be effectively of the order of $2\pi/q_{\mathrm{ISTS}}$ or $1/q_{\mathrm{ISTS}}$ even though the MFP of phonons could become longer outside the thermal grating. Since we have used Eq. (3) with the thermal diffusivity measured in relatively large samples[32,33,39,47] and estimated the values of $\bar{l}$ to be much larger than q_{ISTS}^{-1} in plotting Fig. 12, the ISTS data points circled by the oval in Fig. 12 should be shifted to $q\bar{l} \lesssim 1$ because $\bar{l}$ is not considered to exceed $\approx 1/q_{\mathrm{ISTS}}$ in the ISTS. We consider that the limitation for $\bar{l}$ has also made the measured Γ_{I}/q^2 in the ISTS in Fig. 11 deviate from curves of D_{th} at the lowest temperatures. In fact, the measured γ_{I}'s are almost unchanged from their value at $q\bar{l} \approx 0.3$. This indicates that the effective MFP of phonons for ISTS does remain approximately 4 μm. This is obviously much shorter than the sample boundary dimensions, which can limit the MFP of phonons.

According to the above discussion, we assume that the correct limit for γ_{I} when $q\bar{l} \gg 1$ is determined from the backscattering measurements to be approximately 0.15 to 0.3. For γ_{I} to be constant for large phonon Knudsen number means that Γ_{I} is linearly proportional to q in the collisionless limit

$$\Gamma_{\mathrm{I}} = K\bar{\omega}_B = K\bar{v}q \quad (q\bar{l} \gg 1), \tag{15}$$

where K stands for a number between ~0.15 and ~0.3, i.e., the limiting value of γ_{I}. The linear q dependence of the linewidth appears to contradict the q^2 dependence in the hydrodynamic regime. However, this qualitatively agrees well with the explanation presented in Ref. 15 in terms of light scattering due to two-phonon difference processes from a single phonon branch. In fact, it has been proposed that Γ_{I} should be proportional to the Brillouin frequency of the acoustic phonon modes which are responsible for scattering of light. The limiting value of $K\bar{\omega}_B$ is also quantitatively comparable to the simulated results of the two-phonon difference theory, viz., $\Gamma_{\mathrm{I}} \rightarrow \sim 0.3\bar{\omega}_B$ as $T \rightarrow 0$.[15] Furthermore, the previously reported value of $\Gamma_{\mathrm{I}} \approx 250$ GHz in C (diamond),[14] which was measured at 628 K (=$0.28\Theta_D$) with $q = 5.6 \times 10^7$ m^{-1} ($\theta = 146°$), $\bar{v} = 1.36 \times 10^4$ m/s, and $q\bar{l} \approx 1.9$, gives $\Gamma_{\mathrm{I}} \approx 0.33\bar{\omega}_B$. This is also in good agreement with Eq. (15).

The above discussions show that for any value of phonon Knudsen number

$$\Gamma_{\mathrm{I}} \lesssim 0.3\bar{\omega}_B,$$

i.e., the spectrum of a QELS I does not extend out to the Brillouin peaks in all the phonon regimes. This is an important criterion for a QELS to be classed as type I.

C. An empirical formula for Γ_I

Before we proceed to describing the intermediate phonon regime, we try to fit a function that reproduces the measured γ_{I} values for given $q\bar{l}$'s. The fact that γ_{I} is proportional to $q\bar{l}$ for a small $q\bar{l}$ and is constant for a large $q\bar{l}$ reminds us of a simple test function as

$$\gamma_{\mathrm{I}} = a(1 - e^{-bq\bar{l}}), \tag{16}$$

where a and b are constants to be estimated via least-squares fit. Although we cannot give a physical interpretation for the formula at the present time, this test function does reproduce the behavior of γ_{I} for a wide range of $q\bar{l}$. In fact, we find that

$$\Gamma_{\mathrm{I}} \simeq \begin{cases} ab\bar{v}\bar{l}q^2 & (\text{for } q\bar{l} \ll 1), \\ a\bar{v}q & (\text{for } q\bar{l} \gg 1), \end{cases}$$

i.e., the q^2 and q^1 dependences of Γ_{I} are reproduced, and we could successfully fit Eq. (16) to the measured values of the γ_{I}. The fitting result is shown in Fig. 13. The dashed line is again the theoretical linear function $(1/3)q\bar{l}$. In order to avoid the fitting instability for relatively large values of γ_{I}, we first calculated the common logarithm of γ_{I} values and then fitted the common logarithm of Eq. (16). In addition, we have omitted the artifact data points here, which we have described before in Sec. V B. The least-squares fit produced a standard deviation of approximately 0.1, which indicates that the fit was performed with a reasonably good accuracy in a wide range of γ_{I}.

The best-fit results obtained for the parameters were $a = 0.16 \pm 0.02$ and $b = 1.7 \pm 0.09$. These yield $\Gamma_{\mathrm{I}} \approx 0.28\bar{v}\bar{l}q^2$ for hydrodynamic regime, which is comparable to but slightly smaller than the theoretical $\Gamma_{\mathrm{I}} = (1/3)\bar{v}\bar{l}q^2$. However, as we have described before, fitting only to the measured points in the pure hydrodynamic regime, namely, $q\bar{l} \lesssim 0.001$, has given a better result, viz., $\Gamma_{\mathrm{I}} \approx 0.31\bar{v}\bar{l}q^2$. For the collisionless regime, the best-fit results have given the limiting value of Γ_{I} as $\approx 0.16\bar{\omega}_B$. Since the measured values of γ_{I} actually lie between 0.15 and 0.3, the fitted value of a is, of course, not conclusive. We consider that the value of a may be affected

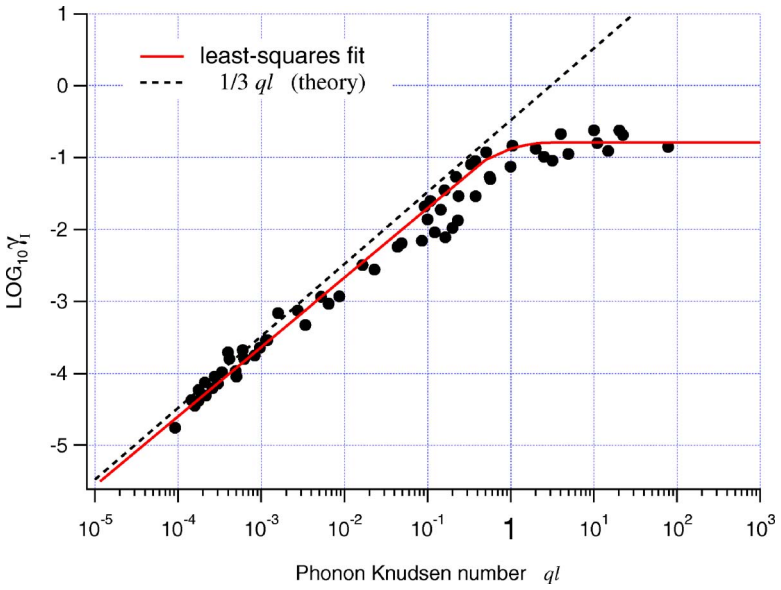

FIG. 13. (Color online) The least-squares fit of common logarithm of Eq. (16) to that of the measured γ_{I} (solid line). The ordinate axis measures the common logarithm of γ_{I}. The dashed line is the linear function $(1/3)q\bar{l}$, which is expected from heat transport theory.

by the choice of $\bar{v}$, i.e., the direction of $\boldsymbol{q}$, or by anisotropy, which we have ignored so far.

D. The intermediate regime

In the intermediate regime, i.e., when $q\bar{l} \approx 1$, γ_{I} is neither proportional to $q\bar{l}$ nor a constant as shown in Figs. 12 and 13. To the best of our knowledge, no light scattering theory for this intermediate phonon regime is available so far. However, we can tell from the fitted curve in Fig. 13 that when $q\bar{l} \simeq 1$

$$\Gamma_{\mathrm{I}} \simeq 0.13\bar{\omega}_B,$$

that is, the linewidth of QELS I in the intermediate phonon regime should lie slightly above $0.1\bar{\omega}_B$. At the present time, we are working on an analysis for our experimental results, employing a novel theory called "extended thermodynamics,"[61] which has been developed recently. This might provide a theoretical formula for γ_{I} against a wide range of $q\bar{l}$, including this intermediate phonon regime. It might also give a physical interpretation for the empirical function (16).

E. The linewidth of QELS II

In Fig. 12, we see that γ_{II} is approximately reciprocally proportional to $q\bar{l}$ for small values of $q\bar{l}$, i.e., at relatively high temperatures, although data for ZnSe have rather large uncertainties. In rutile and $SrTiO_3$, the product of the phonon Knudsen number $q\bar{l}$ and γ_{II} has values between approximately 0.3 and 0.5. This can be explained from the fact that the QELS II has an approximately linear T dependence and little q dependence.[12,15] Since $\bar{l}$ is inversely proportional to T at high temperatures, where QELS II is visible, γ_{II} is considered to be inversely proportional to $q\bar{l}$. However, the origin for the linear-in-T dependence of the QELS II is not clear even now. It should be noted that γ_{II} seems to be larger than unity for all the samples investigated. This indicates that Γ_{II} is always larger than ω_B, and we see that the QELS II is not a consequence of thermodynamic phonon processes because of the discussion made in Sec. V A.

F. On the broad doublet in $SrTiO_3$

Here we discuss on the possibility of second sound for the broad doublet, which has been observed in $SrTiO_3$. Since second sound is a wave of entropy, a light scattering spectrum of second sound should gradually change from an EFLS (or a QELS I) into a doublet with decreasing temperature.[62,63] If the missing QELS I in $SrTiO_3$ below $\sim$70 K was essentially *absent* at low temperatures, then it might imply that the QELS I might, just as theoretically predicted, evolve into the observed broad doublet across the temperature of $\sim$70 K on cooling.

The window condition, which has to be fulfilled for the propagation of second sound, is given in the form[57]

$$\tau_R^{-1} \ll \omega_{\mathrm{SS}} \ll \tau_N^{-1}, \tag{17}$$

where τ_R and τ_N are the mean free time for the resistive (Umklapp plus impurity) and the Normal scattering of phonons, respectively. Hehlen *et al.*[9] have discussed the possibility of second sound for this doublet, but they have reported that they could not estimate τ_R due to the lack of the thermal diffusivity data for an oriented $SrTiO_3$ in the low-T tetragonal phase. However, the effective phonon collision process contributing thermal diffusion is considered to be the resistive process,[23] and therefore our ISTS results now enable us to directly estimate τ_R from Eqs. (5) and (14). Equation (17) can be alternatively written in terms of the phonon Knudsen number as follows:

$$ql_N \ll 1 \ll ql_R, \tag{18}$$

where $l_N = \bar{v}\tau_N$ and $l_R = \bar{v}\tau_R$ are the MFP for the normal and resistive scattering processes, respectively. Here we have assumed that $v_{SS} \approx (1/\sqrt{3})v_{\mathrm{LA}} \approx \bar{v}$, where v_{SS} is the second sound velocity, and this is a reasonably good approximation

for most solids.[57] Equation (18) can be interpreted that collisionless and hydrodynamic regimes are necessary for resistive and normal phonons, respectively.

For the temperature of 15 K in $SrTiO_3$, we obtain a value of MFP as $l_R \approx 1.4 \times 10^{-7}$ m from the measured Γ_I using Eqs. (5) and (14) with $\bar{v}=5500$ m/s. With the value of the wave-vector transfer employed in the backscattering experiment, $q=6.0\times10^7$ m^{-1}, we see that $ql_R=8.4$, which is larger than unity, but not too large as in the case of other materials: in rutile, for example, $ql_R \approx q\bar{l}$ at 20 K is as large as 80. Although accurate estimation for l_N is not available, it is predicted[52] that l_N can be exceptionally shorter than l_R in quantum paraelectrics such as $SrTiO_3$ and $KTaO_3$ due to additional collisions between the soft transverse optic phonons and the acoustic phonons, both of which are long-wave (zone center) phonons and can conserve the quasimomentum. If we assume that $\tau_N \approx (1/10)\tau_R$,[64] ql_N can be estimated to be approximately 0.8, indicating that the window of Eqs. (17) and (18) is slightly open for the backscattering experiment. If we adopt a shorter τ_N or l_N, the window could be more widely open. The "resistive" phonon Knudsen number ql_R in $SrTiO_3$ ranges from 1 to 33 with decreasing temperature from 50 K down to 5 K. If l_N is actually shorter than l_R to a certain degree, this is consistent with the emergence of the broad doublet shown in Fig. 9. Furthermore, our recent analysis in terms of extended thermodynamics[61,65] suggests that even when l_N is comparable to l_R and even when $ql_N \gtrsim 1$, QELS I may change into a doublet spectrum, which can be considered as light scattering by a rather dilute (and overdamped) phonon population similar to second sound.[66] Since the second-sound window is closed in this case, the second sound is not considered to propagate as a well-defined wave. This excitation may, however, still give rise to a spectral doublet instead of a QELS. In such a condition, since both resistive and normal phonons are viewed as in collisionless regime, the scattering of light might be better modeled rather by light scattering due to two-phonon difference processes from a single phonon branch[13,15,55] than by light scattering by second sound.

Recent reports[55,67] do not support the second sound scenario, but they have not completely ruled out its possibility. Furthermore, it seems that they have neither referred to the existence of the EFLS nor have they pointed out the disappearance of the EFLS. With the available data, however, it is hard to decompose the present spectra in $SrTiO_3$ at low temperatures into QELS I, QELS II, and broad doublet for a few reasons. First, Γ_{II} at low temperatures below 70 K is as narrow as $D_{th}q^2$. Second, the spectral tails of the doublet almost overlap that of the QELS II. It is not expected that ISTS in $SrTiO_3$ could detect second sound because the window (18) is located in a range far above unity for a small value of q employed in the ISTS, viz., $1 \ll ql_N, ql_R$. A light scattering experiment with as small scattering angle as $\theta \approx 30^\circ$ may help separate the spectra of the QELS I and the doublet from the QELS II because changing θ does not bring about significant effects on QELS II while it does on QELS I and on the doublet.[9]

VI. SUMMARY

We observed the QELS in the crystals of TiO_2 (rutile), ZnSe, silicon, and $SrTiO_3$. While the QELS II does extend far out to the Brillouin peaks, we have shown that the QELS I never broadens to beyond the Brillouin peaks. By using the backscattering and the ISTS apparatus, we measured the temperature and wave-vector dependences of Γ_I. We have confirmed that the QELS I can be regarded as EFLS and Γ_I exhibits the well-known q^2 dependence in the hydrodynamic phonon regime, i.e., for $q\bar{l} \ll 1$. Although the model of two phonon difference scattering from a single phonon branch has given a linear-in-q dependence for Γ_I in the collisionless phonon regime,[15] the consistency with the thermodynamic q^2 dependence in the hydrodynamic phonon regime had not been discussed. However, we have experimentally confirmed for the first time to the best of our knowledge that the q^2 dependence of Γ_I gradually changes into a q^1 dependence with increasing phonon Knudsen number toward collisionless phonon regime $q\bar{l} \gtrsim 1$. We have found that the limiting linewidth of the QELS I in the collisionless phonon regime is likely to lie around $\sim 0.2\bar{\omega}_B$. It is worth noting that in $SrTiO_3$ Γ_I has been found to be always proportional to q^2, which clearly indicates that there are actually many phonon collisions even at as low temperatures as 40 K in this material. This is an interesting result with regard to the possible existence of second sound in quantum paraelectrics such as $SrTiO_3$ and with regard to the observed broad doublet spectrum,[9,52] on which we have given a brief discussion in terms of phonon Knudsen number. It is also interesting to point out that Γ_I measured in the ISTS also tends to be proportional to q at the lowest temperatures in the ISTS, as has been discussed in Sec. V B. The mechanisms of forming the transient grating and of the diffraction of probe light should be accordingly reconsidered for the case when $\bar{l}$ approaches the pitch of the transient grating because conventional ISTS theories have implicitly assumed only local thermal equilibrium.[20,21]

We have also performed least-squares fit of an empirical function to the measured values of γ_I. The fitting result agrees quite well with the predictions by the heat transport theory and the two-phonon difference scattering theory in the hydrodynamic and collisionless limits, respectively. The result has also allowed us, for the first time to our knowledge, to estimate that QELS I should have a width slightly larger than $\sim(1/10)\bar{\omega}_B$ in the intermediate phonon regime, where $q\bar{l} \simeq 1$.

Further experimental and theoretical studies are necessary to find a rigorous function for Γ_I against arbitrary phonon Knudsen number. This has to be done by extending both macroscopic and microscopic theories: from our ongoing analyses, we feel that the macroscopic extension in terms of extended thermodynamics[61,65] seems to be able to bridge the two limiting phonon regimes. Also further studies are needed to understand the ISTS at low temperatures. The QELS II must be investigated in further detail in connection with the QELS I because the two-component QELS due to phonon-density fluctuations is seemingly universal in dielectric crystals.

ACKNOWLEDGMENTS

The authors wish to gratefully acknowledge Dr. Makoto Mikami, Dr. Jifeng Wang, and Dr. Minoru Isshiki of the Di-

vision of Materials Design, Institute of Multidisciplinary Research for Advanced Materials, Tohoku University, for supplying the pure sample crystals of ZnSe. This research was partially supported by the Ministry of Education, Science, Sports and Culture, Grant-in-Aid for Young Scientists (B), No. 16740165, 2004.

[1] W. D. Johnston and I. P. Kaminow, Phys. Rev. **168**, 1045 (1968).
[2] P. D. Lazay, J. H. Lunacek, N. A. Clark, and G. B. Benedek, *Light Scattering Spectra of Solids* (Springer, Berlin, 1969), p. 593.
[3] P. A. Fleury and K. B. Lyons, Phys. Rev. Lett. **36**, 1188 (1976).
[4] J. R. Sandercock, Solid State Commun. **26**, 547 (1978).
[5] P. A. Fleury and K. B. Lyons, *Light Scattering Near Phase Transitions* (North-Holland, Amsterdam, 1983), Chap. 7.
[6] J. R. Sandercock, *Light Scattering in Solids III* (Springer-Verlag, Berlin, 1982), Chap. 6.
[7] G. J. Coombs and R. A. Cowley, J. Phys. C **6**, 121 (1973).
[8] A. D. Bruce and R. A. Cowley, Adv. Phys. **29**, 219 (1980).
[9] B. Hehlen, A. L. Perou, E. Courtens, and R. Vacher, Phys. Rev. Lett. **75**, 2416 (1995).
[10] F. M. Jiang and S. Kojima, Appl. Phys. Lett. **77**, 1271 (2000).
[11] J. R. Sandercock, Opt. Commun. **2**, 73 (1970).
[12] K. B. Lyons and P. A. Fleury, Phys. Rev. Lett. **37**, 161 (1976).
[13] M. W. Anderson, S. M. Lindsay, and R. T. Harley, J. Phys. C **17**, 6877 (1984).
[14] H. E. Jackson, R. T. Harley, S. M. Lindsay, and M. W. Anderson, Phys. Rev. Lett. **54**, 459 (1985).
[15] A. Koreeda, M. Yoshizawa, S. Saikan, and M. Grimsditch, Phys. Rev. B **60**, 12730 (1999).
[16] P. R. Stoddart and J. D. Comins, Phys. Rev. B **62**, 15383 (2000).
[17] A. Koreeda, Ph.D. thesis, Tohoku University, Sendai, Japan, 1999.
[18] L. D. Landau and E. M. Lifshitz, *Electrodynamics of Continuous Media* (Pergamon, Amsterdam, 1984).
[19] R. D. Mountain, Rev. Mod. Phys. **38**, 205 (1966).
[20] K. A. Nelson, R. J. D. Miller, D. R. Lutz, and M. D. Fayer, J. Appl. Phys. **53**, 1144 (1982).
[21] H. J. Eichler, P. Günter, and D. W. Pohl, *Laser-Induced Dynamic Gratings* (Springer-Verlag, Berlin, 1986).
[22] R. K. Wehner and R. Klein, Physica (Utrecht) **62**, 161 (1972).
[23] C. Kittel, *Introduction to Solid State Physics* (Wiley, New York, 1953).
[24] G. Chen, Phys. Rev. Lett. **86**, 2297 (2001).
[25] R. Vacher, H. Sussner, and S. Hunklinger, Phys. Rev. B **21**, 5850 (1980).
[26] R. Vacher and J. Pelous, Phys. Lett. **53A**, 233 (1975).
[27] R. Vacher and J. Pelous, Phys. Rev. B **14**, 823 (1976).
[28] R. Vacher, J. Pelous, and E. Courtens, Phys. Rev. B **56**, R481 (1997).
[29] A. Akhieser, J. Phys. (USSR) **1**, 277 (1939).
[30] T. O. Woodruff and H. Ehrenreich, Phys. Rev. **123**, 1553 (1961).
[31] *Thermophysical Properties of Matter, The TPRC Data Series*, edited by Y. S. Touloukian (IFI/Plenum, New York, 1970), Vol. 13.
[32] *Thermophysical Properties of Matter, The TPRC Data Series*, edited by Y. S. Touloukian (IFI/Plenum, New York, 1970), Vol. 2.
[33] *Thermophysical Properties of Matter, The TPRC Data Series*, edited by Y. S. Touloukian (IFI/Plenum, New York, 1970), Vol. 5.
[34] W. Hayes and R. Loudon, *Scattering of Light by Crystals* (Wiley, New York, 1978).
[35] N. V. Surovtsev, J. A. H. Wiedersich, V. N. Novikov, E. Rössler, and A. P. Sokolov, Phys. Rev. B **58**, 14888 (1998).
[36] J. Gapiński, W. Steffen, A. Patkowski, A. P. Sokolov, A. Kisliuk, U. Buchenau, M. Russina, F. Mezei, and H. Schober, J. Chem. Phys. **110**, 2312 (1999).
[37] H. C. Barshilia, G. Li, G. Q. Shen, and H. Z. Cummins, Phys. Rev. E **59**, 5625 (1999).
[38] J. Rams, A. Tejede, and J. M. Cabrera, J. Appl. Phys. **82**, 994 (1997).
[39] I. Broser, O. Madelung, H. Weiss, H. J. Schulz, H. E. Gumlich, D. Theis, D. Tshierse, and H. Nelkowski, *Landolt-Börnstein: Zahlenwerte und Funktionen aus Naturwissenschaften und Technik, Neue Serie: Gruppe 3. Kristall- und Festkörperphysik: Band. 17. Halbleiter: Teilband b, Physik der II-VI und I-VII-Verbindungen, Semimagnetische Halbleiter Elemente* (Springer, Berlin, 1982).
[40] T. Toyoda and M. Yabe, J. Phys. D **16**, L251 (1983).
[41] M. H. Grimsditch, Phys. Rev. B **14**, 1670 (1976).
[42] J. R. Harris, G. T. Johnston, G. A. Kepple, P. C. Krok, and H. Mukai, Appl. Opt. **16**, 436 (1977).
[43] J. G. Traylor, H. G. Smith, R. M. Nicklow, and M. K. Wilkinson, Phys. Rev. B **3**, 3457 (1971).
[44] S. Adachi and C. Hamaguchi, Phys. Rev. B **19**, 938 (1979).
[45] B. K. Baĭramov, A. V. Gol'tsev, É. Karaĭamaki, R. Laĭkgo, T. Levola, and V. V. Toporov, Sov. Phys. Solid State **25**, 739 (1983).
[46] E. Käräjämäki, R. Laiho, T. Levola, B. H. Bairamov, A. V. Gol'tsev, and T. Toporov, Phys. Rev. B **29**, 4508 (1984).
[47] T. Mitsui *et al.*, *Landolt Börnstein, Zahlenwerte und Funktionen aus Naturwissenschaften und Technik, Neue Srie Gruppe III: Kristall- und Festkörperphysik, Band 16: Ferroelektrika und verwandte Subustanzen, Teilband a: Oxide* (Springer-Verlag, Berlin, 1981).
[48] D. Moses, A. Talmi, and L. Benguigui, Phys. Rev. B **16**, 533 (1977).
[49] M. C. Gallardo, R. Burriel, F. J. Romero, F. J. Gutiérrez, and E. K. H. Salje, J. Phys.: Condens. Matter **14**, 1881 (2002).
[50] E. F. Steigmeier, Phys. Rev. **168**, 523 (1968).
[51] R. O. Bell and G. Ruprecht, Phys. Rev. **129**, 90 (1963).
[52] V. L. Gurevich and A. K. Tagantsev, Sov. Phys. JETP **67**, 206 (1988).
[53] E. Courtens, Ferroelectrics **183**, 25 (1996).
[54] K. A. Müller, Ferroelectrics **183**, 11 (1996).
[55] E. Farhi, A. K. Tagantsev, B. Hehlen, R. Currat, L. A. Boatner, and E. Courtens, Physica B **276**, 274 (2000).
[56] T. Hasegawa and K. Tanaka, J. Lumin. **94-95**, 15 (2001).
[57] R. A. Guyer and J. A. Krumhansel, Phys. Rev. **148**, 778 (1966).
[58] C. Herring, Phys. Rev. **95**, 954 (1954).
[59] G. P. Srivastava, *The Physics of Phonons* (Adam Hilger, Bristol, 1990).
[60] P. R. Stoddart and J. D. Comins (unpublished).

[61] I. Müller and T. Ruggeri, *Rational Extended Thermodynamics*, 2nd ed. (Springer, Berlin, 1998).
[62] M. Chester, Phys. Rev. **131**, 2013 (1963).
[63] R. H. Enns and R. R. Haering, Phys. Lett. **21**, 534 (1966).
[64] D. W. Pohl and V. Irniger, Phys. Rev. Lett. **36**, 480 (1976).
[65] W. Dreyer and H. Struchtrup, Continuum Mech. Thermodyn. **5**, 3 (1993).
[66] A. Koreeda, S. Ohno, T. Sonehara, E. Tatsu, and S. Saikan (unpublished).
[67] M. Yamaguchi, T. Yagi, Y. Tsujimi, H. Hasebe, R. Wang, and M. Itoh, Phys. Rev. B **65**, 172102 (2002).
[68] From the Akhieser and the Landau-Rumer theories (Ref. 30), the MFP of an acoustic phonon l_B is proportional to ω_B^{-2} and ω_B^{-1} for the lowest and the highest frequency limits ($\omega_B\bar{\tau} \ll 1$ and $\omega_B\bar{\tau} \gg 1$), respectively.
[69] Wehner and Klein have estimated the enhancement factor for silicon to be as much as 20 600 by using photoelastic constants for 3.39 μm wavelength in their report (Ref. 22).